IEEE Photonics Journal
An IEEE Photonics Society Publication

Open Access

Probing Composite Vibrational Fingerprints in the Terahertz Range With Graphene Split Ring Resonator

Volume 12, Number 5, October 2020

Xinrong Mao
Yanfen Hang
Yuanguo Zhou
Jinfeng Zhu
Qiang Ren
Jianming Zhuo
Yijun Cai

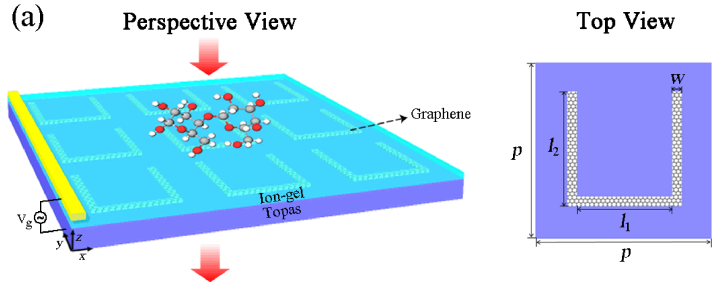

DOI: 10.1109/JPHOT.2020.3017375

IEEE photonics SOCIETY
IEEE

Probing Composite Vibrational Fingerprints in the Terahertz Range With Graphene Split Ring Resonator

Xinrong Mao,[1] Yanfen Hang,[1] Yuanguo Zhou,[1] Jinfeng Zhu,[2] Qiang Ren,[3] Jianming Zhuo,[4] and Yijun Cai[5,6]

[1]College of Communication and Information Engineering, Xi'an University of Science and Technology, Xi'an 710054, China
[2]Department of Electronic Science, Xiamen University, Xiamen 361005, China
[3]School of Electronics and Information Engineering, Beihang University, Beijing 100191, China
[4]Xiamen Blue Ocean Technology Company Limited, Xiamen 361022, China
[5]Fujian Provincial Key Laboratory of Optoelectronic Technology and Devices, Xiamen University of Technology, Xiamen 361024, China
[6]Key Laboratory of Microelectronic Devices & Integrated Technology Institute of Microelectronics, Chinese Academy of Sciences, Beijing 100191, China

DOI:10.1109/JPHOT.2020.3017375

Manuscript received July 22, 2020; revised August 11, 2020; accepted August 14, 2020. Date of publication August 18, 2020; date of current version August 31, 2020. This work was supported in part by the Natural Science Basic Research Plan in Shaanxi Province of China under Grant 2020JM-515 and in part by the Opening Project of Key Laboratory of Microelectronic Devices & Integrated Technology, Institute of Microelectronics, Chinese Academy of Sciences; NSAF (U18301160). Corresponding authors: Yuanguo Zhou; Yijun Cai (e-mail: wingkoo@foxmail.com; yijuncai@foxmail.com).

Abstract: Sensors with single resonant mode often produce false positive when detecting the composite vibrational fingerprints of molecules in the terahertz (THz) range. In this study, a multi-resonant plasmonic structure, consisting of periodic graphene split ring resonator (SRR) arrays, is proposed for THz sensing. The effective detection of ultrathin (0.1 μm) lactose layer is given as an example to demonstrate the detection sensitivity. The vibrational fingerprints of lactose at 0.53 THz and 1.37 THz are enhanced in transmission spectra. Besides, resonant frequencies could be actively adjusted with the gate voltage applied on the SRR array. The physical mechanism of multi-resonance can be explained by a combination of LC resonance and dipole resonance of the structure, which can be observed in the electric field distributions. Moreover, the sensing performance can be further optimized by varying geometric parameters. Furthermore, the refractive index sensing performance of the sensor is also investigated by altering the surrounding medium on the surface. The designed sensor can work under an oblique incidence, which provides potential applications in biological analysis and medical diagnostics.

Index Terms: Terahertz sensing, split ring resonator, graphene, surface plasmons.

1. Introduction

Terahertz (THz) wave has wide application prospects in the field of sensing due to its unique properties, such as transparency in most media, non-ionization characteristics, and low photon energy [1]–[3]. Moreover, vibrational resonances of various molecules are located in the THz range, which provides a new idea for the design of molecular fingerprint detection sensors [4]. However,

compared with THz scale (ranging from tens to hundreds of micrometers in wavelength), the size of most molecules (several nanometers in diameter) is extremely small, resulting in very weak interaction between molecules and THz wave. Therefore, a large volume of samples are often required to identify specific molecules. To overcome this limitation, it is necessary to enhance the interaction between light and molecules, thus improving the sensitivity of the THz detection technology.

In order to obtain obvious vibrational signal with a small volume of samples, researchers utilized microstructures or nanostructures to enhance the local electric field for improving the detection sensitivity. For example, nano-antenna array, metallic gratings and split ring resonator have been used to achieve the localized field enhancement, increasing the absorption cross section of the molecules [5]–[7]. On the other hand, the waveguide structures have the advantage of increasing the effective interaction length between molecules and THz waves for the same volume of sample [8]. Nevertheless, in the above reported methods, the sensors consisting of traditional noble metals are difficult to tune after fabrication. Therefore, other tunable materials should be taken into consideration to adjust the resonant characteristics.

Graphene has attracted extensive attentions of researchers [9]–[15]. By applying bias voltage to adjust its Fermi level, the conductivity of graphene can be tuned to support surface plasmon polariton (SPP) in THz range. At the same time, graphene-based sensors tend to have better detection sensitivity due to the strong light confinement capacity of graphene. Rodrigo *et al*. proposed a biosensor based on graphene nanoribbons for the label-free detection of proteins [16]. The plasmonic resonances were dynamically adjusted by applying bias voltage on graphene so as to selectively overlap with different vibrational bands of proteins. Wu *et al*. reported a biosensor with a continuous graphene layer integrated on top of a gold grating to identify nanometric molecules, and showed that tunable graphene plasmons can accurately resolve the fingerprint of the target molecule [17]. Nevertheless, all of the graphene-based sensors mentioned above have an individual resonance, showing limitation in identifying spectrally separated vibrational fingerprints of molecules. When the multiple vibrational fingerprints in analytes are spectrally separated, sensors with single resonance mode are unable to identify them simultaneously. Therefore, false positive usually occurs in the detection for analytes with multiple vibrational fingerprints using sensors with single resonance mode.

In our previous study, the multi-resonant sensing configurations require the combination of unit cells with different geometric parameters to produce diverse dipole resonances [18]. In this paper, we utilize the unit cell with unique geometric parameter to obtain multi-resonance thus simplifying the processing. We numerically study a multi-resonant sensor based on graphene SRR metasurface, which can be utilized to realize fingerprint detection in the THz range. By changing the gate voltage, the resonant frequency of the plasmonic structure can be dynamically adjusted so that it overlaps with the vibrational fingerprints of lactose molecules. The effect of geometric parameters on sensor performance will be investigated as well. Besides, while the thickness of analyte is fixed as 0.1 μm, the proposed sensor exhibits different sensing sensitivities for respective resonance (0.03 THz/RIU for the left and 0.10 THz/RIU for the right resonance). The influence of the incident angle and polarization angle on the sensing performance will also be discussed.

2. Modeling and Methods

Fig. 1(a) illustrates the schematic diagram of the proposed sensor, which is composed of an array of graphene SRR on the top of cyclic olefin copolymer (Topas) substrate with a thickness of $t = 4.0$ μm [19]. In our proposed device, a Topas layer is usually deposited onto a silicon wafer. Graphene is grown using chemical vapour deposition on copper and transferred onto the Topas substrate. Graphene SRR arrays can be fabricated by using standard optical lithography followed by oxygen plasma etching. A layer of ion-gel can be spin-coated on the graphene patterns and contacted to the Au electrodes as the top gate. Other geometric parameters of the unit cell are as follows: the periodic length $p = 18.0$ μm, the line width $w = 0.7$ μm, the inner side length $l_1 = 11.0$ μm, the outer side length $l_2 = 12.4$ μm ($l_2 = l_1 + 2 \times w$). The relative permittivity of Topas is

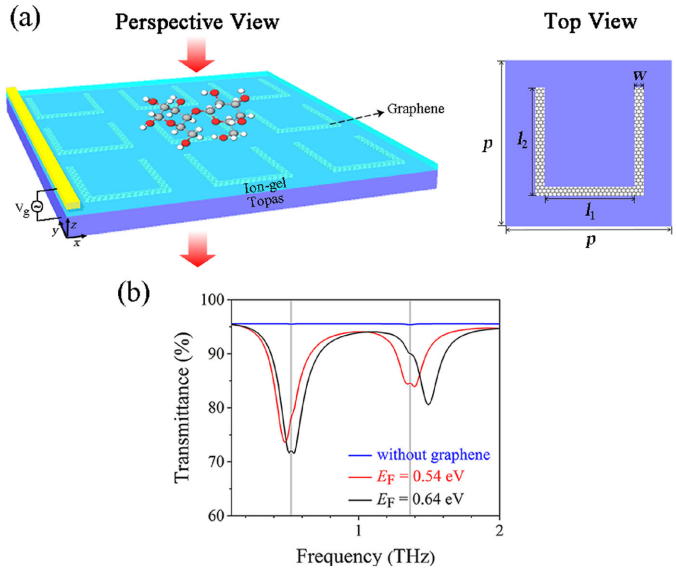

Fig. 1. (a) Schematic of graphene SRR sensor. p is the periodic length. w is the line width of SRR. l_1 and l_2 denote the side lengths of the inner and outer SRR, respectively. (b) Transmission spectra of the graphene SRR array (red and black curves) and bare Topas substrates (blue curves) covered with 0.1 μm lactose, respectively. The gray vertical bars represent the vibrational bands of lactose molecule.

chosen as 2.35 [20]. In addition, considering the way of modulating the Fermi energy of graphene, an ion-gel-gated method is used here to achieve a large-scale modulation of the graphene Fermi energy. The ion-gel is modeled as a layer of homogenous material with a non-dispersive permittivity of 1.82 and a thickness of 100 nm according to Ref [21], [22]. We assume that the THz plane wave illuminates upon the top of the structure vertically, and interacts with the adsorbed biomolecules and the graphene metasurface. Finite element method (FEM) is used to simulate the transmission characteristics of the proposed structure. In the simulation, the periodic boundary conditions are applied in the x- and y-directions, and the Floquet ports are applied in the z-direction. Triangular meshes of user-defined size are applied on graphene layers due to their localized enhanced electromagnetic fields. Tetrahedral meshes are applied for the remaining domains of the structure.

In this paper, graphene is modeled as a two-dimensional conductive surface with zero thickness. In the THz region, the intraband contribution dominates the graphene conductivity, and the inter-band transition can be negligible. At $T = 300$ K, the conductivity of graphene can be obtained from the following simplified Kubo formula [23]:

$$\sigma_g = \frac{ie^2 E_F}{\pi\hbar^2(\omega + i\tau^{-1})} \tag{1}$$

where ω is the angular frequency, E_F is the Fermi energy, $\hbar$ is the reduced Planck constant, τ is the electron-phonon relaxation time, e is the charge of electron.

In order to guarantee the accuracy and the validity of the simulation model, according to the previous work from [24], τ is chosen as 1 ps in the following simulations. The relation between E_F and the voltage bias V_g is given as follows [25]:

$$E_F = \hbar v_f \sqrt{\frac{\pi \varepsilon_0 \varepsilon_r V_g}{eD}} \tag{2}$$

where v_f is the Fermi velocity, ε_0 is the permittivity of free space, ε_r is the relative permittivity of the spacer and D is the thickness of insulating layers.

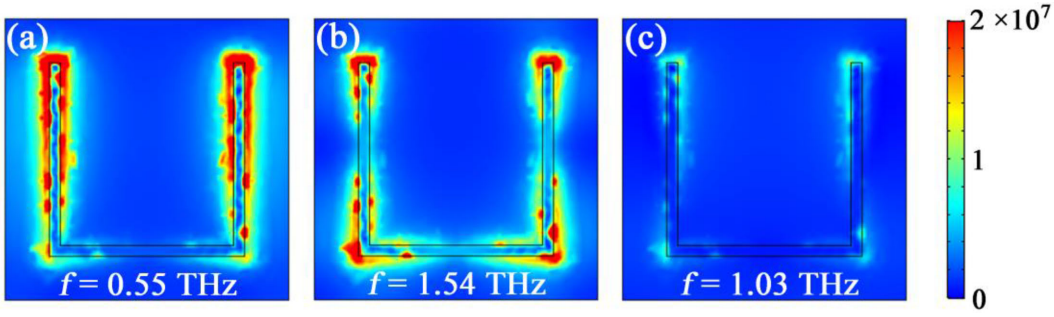

Fig. 2. Electric field distributions of graphene SRR sensor with lactose at (a) $f = 0.55$ THz, (b) $f = 1.54$ THz, and (c) $f = 1.03$ THz under normal TE incidence.

3. Results and Discussion

In order to investigate the molecular detection capability of the graphene SRR sensor, we choose lactose as the analyte, as it showed strong vibrational resonance at 0.53 THz and 1.37 THz. Lorentzian mode is used to model the permittivity of lactose to illustrate its absorption features as follows [26]:

$$\varepsilon_r = \varepsilon_\infty + \sum_{p=1}^{\infty} \frac{\Delta\varepsilon_p w_p^2}{\omega_p^2 - \omega^2 - j\gamma_p w} \tag{3}$$

where ε_∞ represents the off-resonance background permittivity of lactose, γ_p and ω_p are the damping rate and the angular frequency of each absorption oscillation. $\Delta\varepsilon_p$ is the oscillation strength factor. The relevant parameters of lactose permittivity are derived from previous experimental work [27].

To verify the effect of the graphene SRR array on the performance, its transmission spectra covered with lactose are plotted compared with that of a bare Topas substrate with lactose deposition, as shown in Fig. 1(b). For bare Topas substrate (without graphene) covered with lactose samples, only slight dips in the transmission spectra at the vibrational resonances of lactose are observed. This is due to a weak interaction between incident light and the ultrathin (0.1 μm) lactose in this frequency range. However, for graphene SRR array covered with lactose layer, obvious transmission peaks at the vibrational resonances of lactose are observed, as shown in Fig. 1(b). This phenomenon is caused by the coupling between plasmonic resonance of the structure and the vibrational resonance of the molecular bonds inside lactose. As can be seen from the Fig. 1(b), when $E_F = 0.64$ eV (black curve), the left resonance of the structure overlaps with the vibrational resonance of lactose at $f = 0.53$ THz, while $E_F = 0.54$ eV (red curve), the right resonance of the structure overlaps with the vibrational resonance of lactose at $f = 1.37$ THz.

To better illustrate the resonance characteristics of graphene SRR array and lactose, we also plot the electric field distributions in Fig. 2. For the left resonance peak ($f = 0.55$ THz), it is obvious that the electric field is mainly concentrated on the arms of SRR, which is caused by LC resonance excitation of graphene SRR array [28], as shown in Fig. 2(a). For the right resonance peak ($f = 1.54$ THz), electric fields are mainly concentrated at the corners of SRR as plotted in Fig. 2(b), which is the result of dipole resonance excitation of graphene SRR array. Fig. 2(a) and 2(b) show that the concentrated electric fields caused by LC resonance and dipole resonance enlarge the absorption cross sections of lactose molecules. In contrast, as shown in Fig. 2(c), the structure has no obvious enhanced electric field at $f = 1.03$ THz. This can be explained by that the two resonant frequencies of the graphene SRR mentioned above are far away from this frequency.

In addition, for metal devices, the resonant frequency is fixed after the structure is manufactured. However, for graphene devices, the resonant frequency can be adjusted by changing the Fermi

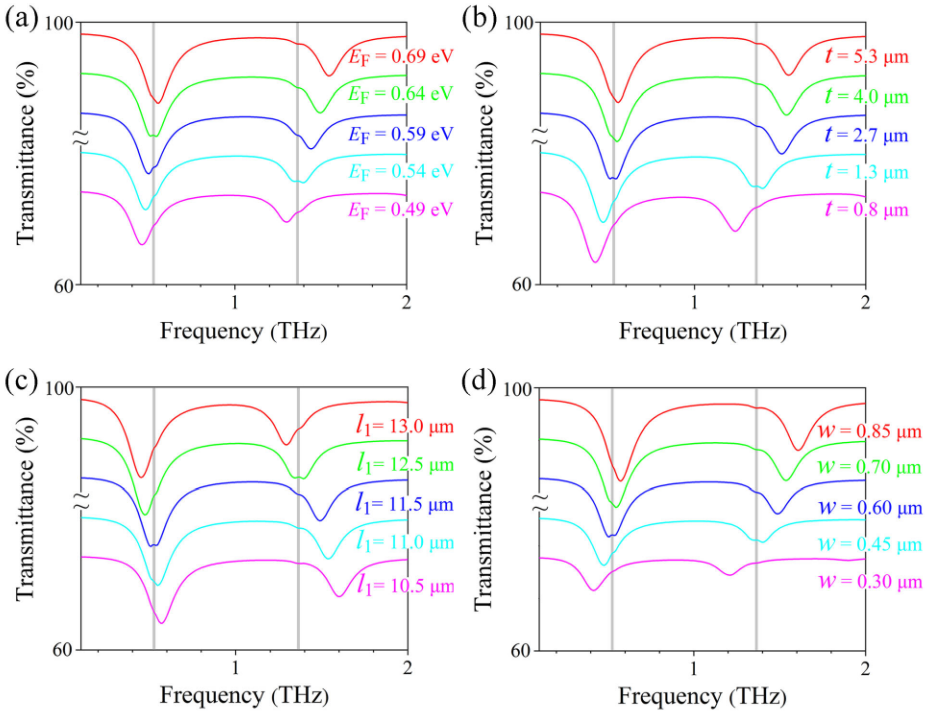

Fig. 3. Transmission spectra of graphene SRR sensor covered with lactose for different E_F, t, l_1 and w under normal TE incidence, where $p = 18$ μm. (a) E_F changes from 0.49 eV to 0.69 eV when $w = 0.7$ μm, $l_1 = 11.0$ μm, $t = 4.0$ μm. (b) t changes from 0.8 μm to 5.3 μm when $w = 0.7$ μm, $l_1 = 11.0$ μm, $E_F = 0.68$ eV. (c) l_1 changes from 10.5 μm to 13.0 μm when $w = 0.7$ μm, $t = 4.0$ μm, $E_F = 0.68$ eV. (d) w changes from 0.30 μm to 0.85 μm when $l_1 = 11.0$ μm, $t = 4.0$ μm, $E_F = 0.68$ eV. The gray vertical bars represent the vibrational bands of lactose molecules. Curves with larger E_F, t, l_1, w are shifted 10% upward to show the spectrum shift more clearly.

energy of the graphene without altering the size of the structure [29], [30]. Therefore, we study the transmission spectra of the sensor with the change of E_F, as plotted in Fig. 3(a). As E_F increases from 0.49 eV to 0.69 eV, the left resonant frequency has a blue shift from 0.50 THz to 0.56 THz and the right resonant frequency shows a blue shift from 1.30 THz to 1.54 THz. In Fig. 3(a), two resonances are tuned with gate voltage *Vg* to sweep through the vibrational bands of lactose. The vibrational signal of lactose can be hardly detected while the vibrational bands of lactose are far away from the plasmonic resonances excited by graphene SRR array.

In fact, the sensing performance of the graphene SRR sensor is closely related to the geometric parameter. Fig. 3(b) depicts that varying the thickness of Topas substrate not only causes the resonances shift but also change the transmission rate. By delicately optimizing the thickness of Topas t, the relatively strong vibrational signal for lactose can be obtained. Fig. 3(c) shows the transmission spectra of different inner side lengths l_1. As l_1 increases from 10.5 μm to 13.0 μm, the left transmission dip has a red shift from 0.57 THz to 0.45 THz, while the right resonance shows an obvious red shift from 1.60 THz to 1.30 THz. Moreover, with the decrease of l_1, the SRR arm spacing is gradually shortened, which may lead to the enhancement of the induced dipole resonance. In Fig. 3(d), one can see that as w increases from 0.30 μm to 0.85 μm, the left resonant frequency exhibits a blueshift from 0.41 THz to 0.58 THz, and right resonant frequency is blue-shifted from 1.21 THz to 1.61 THz. On the other hand, as w increases, the duty cycle of graphene coverage increases, leading to the increase of energy dissipation inside graphene and the decrease of transmission rate.

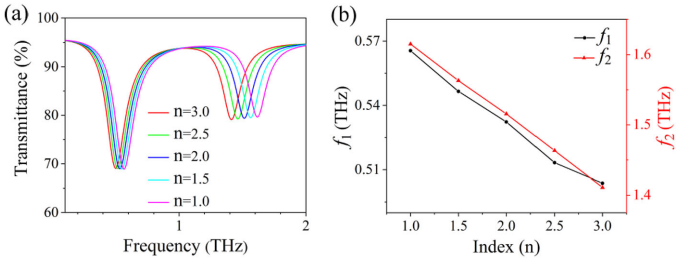

Fig. 4. (a) Transmission spectra of the graphene SRR sensor covered with analytes of different refractive indices. (b) The left resonant frequency f_1 (black curve) and the right resonant frequency f_2 (red curve) as a function of the detected refractive index.

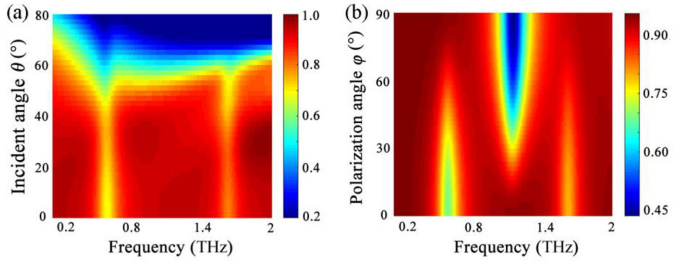

Fig. 5. (a) Dependence of the transmission spectra on the incident angle θ for TE polarization. (b) Transmission spectra as a function of the polarization angle φ under normal incidence.

Next, in order to investigate the refractive index (RI) sensing performance of graphene SRR sensor, we apply an analyte layer on the surface of the sensor with a thickness of 0.1 μm. Here, the corresponding structure parameters are $p = 18.0$ μm, $w = 0.7$ μm, $l_1 = 11.0$ μm, $t = 4.0$ μm, $E_F = 0.68$ eV. As the surrounding medium adsorbed on the surface of sensor is altered, the resonant properties of graphene SRR sensor will be changed, which can be utilized for RI sensing applications. Fig. 4(a) shows the relationship between the transmission spectra and the RI of analytes. The RI is selected as a value from 1.0 to 3.0, which covers a large number of important materials in the THz band. As depicted in Fig. 4(a), the left resonant frequency f_1 and the right resonant frequency f_2 both have a red shift gradually with the increase of RI. In addition, the frequency shift of f_2 is more obvious than that of f_1. For example, when RI varies from 1.0 to 3.0, the frequency shift of f_2 is 0.20 THz, while that of f_1 is only 0.07 THz. According to the proposed calculation method in Ref [31], we also obtain the dephasing time as 11.1 ps for the left resonance at 0.56 THz, and 11.8 ps for the right resonance at 0.62 THz. Fig. 4(b) depicts the corresponding resonant frequency for each transmission dip as a function of the detected RI. Sensor sensitivity is usually quantified as $S = \Delta f / \Delta n$ (in Hz per refractive index unit, Hz/RIU). The sensitivities of the left resonance and the right resonance are approximately 0.03 THz/RIU and 0.10 THz/RIU, respectively. The sensitivity of the right resonance is higher than that of the sensor based on InSb-based metallic gratings for lactose molecular detection (0.06 THz/RIU) [6]. The sensing accuracy for the analyte is significantly improved due to the strong confinement of local electromagnetic fields around graphene.

In the above study, the performance of graphene SRR sensor has been investigated with the electric field along *x*-direction under normal incidence. Finally, the dependence of this structure on incident angle θ and polarization angle φ will be studied under the same parameter conditions as in Fig. 4. Fig. 5(a) shows the transmission spectra as a function of the incidence angle θ under TE polarization. When θ is smaller than 70°, two resonances can be observed at 0.55 THz and 1.54 THz, indicating that the variation of incident angle in a wide range has little effect on the multi-resonant sensing performance of the structure. The dependence of the transmission spectra

on the polarization angle φ under normal incidence is shown in the Fig. 5(b). Obviously, with the polarization angle φ increasing from 0° to 90°, the transmission spectra of the structure is greatly affected by the polarization angle. As can be seen from Fig. 5(b), when φ is less than 12°, two resonances can be observed at 0.55 THz and 1.54 THz, respectively. As φ increases from 12° to 78°, a new resonance appears at 1.20 THz, forming three resonances at three specific frequencies However, when φ is greater than 78°, only a single resonance exists at 1.20 THz. The polarization dependence is mainly caused by the asymmetry of the structure.

4. Conclusion

In summary, we have designed a plasmonic structure for THz sensing using periodic graphene SRR, whose resonances can be tuned by electrostatic gating. Due to the strongly localized electric field induced in the graphene SRR array, the coupling effect between plasmonic resonance and vibrational resonance inside lactose molecules is significantly enhanced, which enabled highly sensitive detection. At the same time, geometric parameters play an important role in the performance of graphene SRR sensor. The refractive index sensing performance of the sensor is also investigated in detail. Numerical results show that the spectral response is highly sensitive to the environmental refractive index, which can achieve a sensitivity of 0.10 THz/RIU. Finally, the effects of the incident angle and polarization angle on sensing performance are also discussed. We believe that our design will provide meaningful guidance for the graphene-based multi-resonant THz sensors.

References

[1] B. Ferguson, and X. C. Zhang, "Materials for terahertz science and technology," *Nature Mater.*, vol. 1, no. 1, pp. 26–33, 2002.

[2] A. Ahmadivand, B. Gerislioglu, R. Ahuja, and Y. K. Mishra, "Terahertz plasmonics: The rise of toroidal metadevices towards immunobiosensings," *Mater. Today*, vol. 32, pp. 108–130, 2020.

[3] B. Gerislioglu, A. Ahmadivand, and N. Pala, "Tunable plasmonic toroidal terahertz metamodulator," *Phys. Rev. B*, vol. 97, no. 16, 2018, Art. no. 161405.

[4] M. R. Leahy-Hoppa, M. J. Fitch, X. Zheng, L. M. Hayden, and R. Osiander, "Wideband terahertz spectroscopy of explosives," *Chem. Phys. Lett.*, vol. 434, no. 4–6, pp. 227–230, 2007.

[5] H. R. Park, K. J. Ahn, S. Han, Y. M. Bahk, N. Park, and D. S. Kim, "Colossal absorption of molecules inside single terahertz nanoantennas," *Nano Lett.*, vol. 13, no. 4, pp. 1782–1786, 2013.

[6] S. Lin, K. Bhattarai, J. Zhou, and D. Talbayev, "Thin InSb layers with metallic gratings: A novel platform for spectrally-selective THz plasmonic sensing," *Opt. Express*, vol. 24, no. 17, pp. 19448–19457, 2016.

[7] B. Han, Z. Han, J. Qin, Y. Wang, and Z. Zhao, "A sensitive and selective terahertz sensor for the fingerprint detection of lactose," *Talanta*, vol. 192, pp. 1–5, 2019.

[8] X. Shi, J. Qin, and Z. Han, "Enhanced terahertz sensing with a coupled comb-shaped spoof surface plasmon waveguide," *Opt. Express*, vol. 25, no. 1, pp. 278–283, 2017.

[9] S. Xiao, T. Wang, T. Liu, X. Yan, Z. Li, and C. Xu, "Active modulation of electromagnetically induced transparency analogue in terahertz hybrid metal-graphene metamaterials," *Carbon*, vol. 126, pp. 271–278, 2018.

[10] X. Luo, Z. Liu, L. Wang, J. Liu, and Q. Lin, "Tunable ultra-narrowband and wide-angle graphene-based perfect absorber in the optical communication region," *Appl. Phys. Express*, vol. 11, no. 10, 2018, Art. no. 105102.

[11] S. Quader, J. Zhang, M. R. Akram, and W. Zhu, "Graphene-based high-efficiency broadband tunable linear-to-circular polarization converter for terahertz waves," *IEEE J. Sel. Topics Quant.*, vol. 26, no. 5, Sep.-Oct. 2020, Art. no. 4501008.

[12] A. Ahmadivand, B. Gerislioglu, and Z. Ramezani, "Gated graphene island-enabled tunable charge transfer plasmon terahertz metamodulator," *Nanoscale*, vol. 11, no. 17, pp. 8091–8095, 2019.

[13] Y. Cai, K. D. Xu, N. Feng, R. Guo, H. Lin, and J. Zhu, "Anisotropic infrared plasmonic broadband absorber based on graphene-black phosphorus multilayers," *Opt. Express*, vol. 27, no. 3, pp. 3101–3112, 2019.

[14] Y. Cai, J. Zhu, and Q. H. Liu, "Tunable enhanced optical absorption of graphene using plasmonic perfect absorber," *Appl. Phys. Lett.*, vol. 106, no. 4, 2015, Art. no. 043105.

[15] H. Li, C. Ji, Y. Ren, J. Hu, M. Qin, and L. Wang, "Investigation of multiband plasmonic metamaterial perfect absorbers based on graphene ribbons by the phase-coupled method," *Carbon*, vol. 141, pp. 481–487, 2019.

[16] D. Rodrigo *et al.*, "Mid-infrared plasmonic biosensing with graphene," *Science*, vol. 349, no. 6244, pp. 165–168, 2015.

[17] T. Wu, Y. Luo, and L. Wei, "Mid-infrared sensing of molecular vibrational modes with tunable graphene plasmons," *Opt. Lett.*, vol. 42, no. 11, pp. 2066–2069, 2017.

[18] Y. Cai, Y. Hang, Y. Zhou, J. Zhu, J. Yang, and X. Wang, "Graphene-based biosensors for detection of composite vibrational fingerprints in the Mid-infrared region," *Nanomaterials*, vol. 9, no. 10, 2019, Art. no. 1496.

[19] L. Maiolo *et al.*, "Quarter-wave plate metasurfaces on electromagnetically thin polyimide substrates," *Appl. Phys. Lett.*, vol. 115, 2019, Art. no. 241602.

[20] P. D. Cunningham *et al.*, "Broadband terahertz characterization of the refractive index and absorption of some important polymeric and organic electro-optic materials," *J. App. Phys.*, vol. 109, no. 4, 2011, Art. no. 043505.
[21] S. Xiao, T. Wang, Y. Liu, C. Xu, X. Han, and X. Yan, "Tunable light trapping and absorption enhancement with graphene ring arrays," *Phys. Chem. Chem. Phys.*, vol. 18, no. 38, 2016, Art. no. 26661.
[22] Z. Fang *et al.*, "Active tunable absorption enhancement with graphene nanodisk arrays," *Nano Lett.*, vol. 14, no. 1, pp. 299–304, 2014.
[23] G. W. Hanson, "Dyadic Green's functions and guided surface waves for a surface conductivity model of graphene," *J. Appl. Phys.*, vol. 103, no. 6, pp. 1–8, 2008.
[24] J. Diaz, M. Morote, and J. Carrier, "Plane wave excitation-detection of non-resonant plasmons along finite-width graphene strips," *Opt. Express*, vol. 21, no. 21, pp. 24856–24872, 2013.
[25] J. S. Gómez-Díaz, and J. Perruisseau-Carrier, "Graphene-based plasmonic switches at near infrared frequencies," *Opt. Express*, vol. 21, no. 13, pp. 15490–15504, 2013.
[26] G. P. Kniffin, and L. M. Zurk, "Model-Based material parameter estimation for terahertz reflection spectroscopy," *IEEE Trans. Terahertz Sci. Technol.*, vol. 2, no. 2, pp. 231–241, Mar. 2012.
[27] A. Roggenbuck *et al.*, "Coherent broadband continuous-wave terahertz spectroscopy on solid-state samples," *New J. Phys.*, vol. 12, no. 4, 2010, Art. no. 043017.
[28] H. Li, M. Qin, Y. Ren, and J. Hu, "Angle-independent strong coupling between plasmonic magnetic resonances and excitons in monolayer WS_2," *Opt. Express*, vol. 27, no. 16, pp. 22951–22959, 2019.
[29] J. Zhang, X. Wei, M. Premaratne, and W. Zhu, "Experimental demonstration of electrically tunable broadband coherent perfect absorber based on graphene-electrolyte-graphene sandwich structure," *Photon. Res.*, vol. 7, no. 8, pp. 868–874, 2019.
[30] J. Zhang, X. Wei, I. D. Rukhlenko, H.-T. Chen, and W. Zhu, "Electrically tunable metasurface with independent frequency and amplitude modulations," *ACS Photon.*, vol. 7, no. 1, pp. 265–271, 2020.
[31] A. Ahmadivand, R. Sinha, B. Gerislioglu, M. Karabiyik, N. Pala, and M. Shur, "Transition from capacitive coupling to direct charge transfer in asymmetric terahertz plasmonic assemblies," *Opt. Lett.*, vol. 41, no. 22, pp. 5333–5336, 2016.